73rd Conference of the Italian Thermal Machines Engineering Association (ATI 2018), 12-14 September 2018, Pisa, Italy

Experimental assessment of spark and corona igniters energy release

G. Discepoli[a,*], V. Cruccolini[a], M. Dal Re[b], J. Zembi[a], M. Battistoni[a], F. Mariani[a], C. N. Grimaldi[a]

[a]Department of Engineering, Università degli Studi di Perugia, Via G. Duranti 95, Perugia 06125, Italy
[b]Federal-Mogul Powertrain Group

Abstract

The Radio-Frequency (RF) Corona Ignition System is an innovative and promising technology able to produce multiple streamers to ignite the fuel throughout the combustion chamber. This system, compared to a conventional spark ignition system, involves wider initial combustion volumes and allows the engine to operate in stable conditions at leaner mixtures, higher EGR dilutions, with faster burning rates and enabling advanced combustion strategies. Due to the intrinsic operating features of the RF corona ignition system, the production of a plasma generated by a high frequency electrical field, the energy released to the surrounding medium is a fundamental parameter to understand its behaviour and impact on a given air-fuel mixture.

The aim of this paper is the energetic characterization of a prototype of corona igniter, called Advanced Corona Ignition System (ACIS), by measuring the pressure increase caused by the streamers in a controlled environment, a pressure based calorimeter. The ACIS results are also compared with a multiple spark discharges (MSD) ignition system based on standard Federal Mogul spark plug technology characterized by an integrated electronics capable of managing up to 17 consecutive discharges. The energy evaluation was carried out at room temperature with air at different pressure levels, up to 10 bar.

Keywords: Energy; Corona effect; Igniter; Lean combustion; Experimental

1. Introduction

Modern engine technology targets are to improve the energy conversion efficiency and reduce exhaust emissions of the combustion system for given operating conditions. To succeed in exploiting ultra lean air-fuel mixture combustion, opportunities are offered by applying innovative systems based on low temperature plasma-assisted ignition [1, 2].

These innovative ignition systems, by means of different ion and excited species production mechanisms, add new paths to start a reaction chain that leads to combustion [3]. Furthermore, transient plasma showed to accelerate the

---

*Corresponding author. Tel.: +39-075-585-3749.
E-mail address: gabriele.discepoli@unipg.it

early combustion phase and, more in general, improve engine performance thanks to the multiple spread ignition locations in the areas of greatest active species production [4, 5]. The oxygen, in atomic, ionic or excited state, seems to be the key chemical species for the plasma ignition [6, 7]. Engine combustion results stabilized and the lean limit is extended with respect to the conventional spark igniter [8, 9]. Also, it has been proved that the low temperature plasma can extend the EGR dilution tolerance [10, 11].

At present, there are only few attempts to model the plasma ignition process because of challenging issues due to the plasma formation timescale, which is orders of magnitude smaller than the ignition process timescale [12].

From a general point of view, the thermal energy delivered to the air-fuel mixture is a key parameter as it heavily affects the flame kernel formation and then the production of a correct ignition [13]. The aim of the present work is to assess the thermal energy released to the medium by the streamers produced by an RF Corona Ignition System and, then, to compare it with the energy released by a conventional system. This investigation concerning low temperature plasma ignition systems has not been reported in the literature yet, to the best of authors' knowledge. Indeed, even if the production of the ion and excited states that starts and promotes the combustion is supposed to be the main feature of the low temperature plasma produced by the ACIS, these chemical activities cannot be separated from the thermal phase that, actually, is spatially distributed, enhancing the chemical kinetics of the exothermic fuel oxidation, resulting in the combustion initiation [4]. Therefore, it is essential to measure and assess the deposited thermal energy.

To this end, the thermal energy delivered by the ignition systems is measured in a simplified and controllable environment, i.e. a constant volume cylindrical vessel, operated at different pressures. Furthermore, the primary electrical energy supplied to the ignition systems is also measured (for the conventional igniter) or calculated (for the ACIS) to address how much of the electrical energy supplied to the igniter is transmitted to the chamber medium.

Nomenclature

ACIS	Advanced Corona Ignition System
MSD	Multiple Spark Discharges
V_{off}	Supply Voltage Offset
E_{PS}	Energy Supplied to the Primary circuit
E_{TR}	Thermal Energy Released to the medium
σ_{PS}^{E}	Standard deviation of the E_{PS} data distribution
σ_{TR}^{E}	Standard deviation of the E_{TR} data distribution
η_E	Electric efficiency
$P_{chamber}$	Pressure in the bomb chamber

---

2. Experimental set-up and methodology

2.1. Test-bench description

The experimental campaign is carried out using a constant volume vessel to allow free management of the operating conditions as pressure, temperature, gas type, volume and geometry. The inner bomb volume ($22.5 \cdot 10^3 \ mm^3$) is made out of Plexiglas for its low thermal conductivity ($0.187 \ W \cdot m^{-1} K^{-1}$) and to allow optical access.

The bomb works as a calorimeter, equipped with a piezoelectric low-pressure sensor (Kistler Type 7261, sensitivity of 2200 $pC \cdot bar^{-1}$, max pressure resolution of $\approx 10^{-5} \ bar$) to measure the energy released in the chamber to the medium by the streamers. The pressure sensor and the igniter tip (fig. 1.a) are mounted opposed to each other (fig. 1.b). The charge signal produced by the pressure sensor is amplified and converted to a proportional voltage signal by a charge amplifier (*Kistler Type 5011*) and then acquired by a fast oscilloscope (*Teledyne LeCroy Wavesurfer 3000*). The oscilloscope also collects the signals produced by a thermocouple which monitors the chamber temperature, by a current probe (*Teledyne LeCroy CP030*, sensitivity of 10 $mA \cdot div^{-1}$) and by a *Teledyne LeCroy PP020* passive probe. In the case of the single or multi-spark tests, the electrical energy supplied to the primary circuit is estimated

by measuring voltage and current simultaneously. These measurements allow to accurately assess how much of the supplied energy is converted and deposited in the medium as thermal energy.
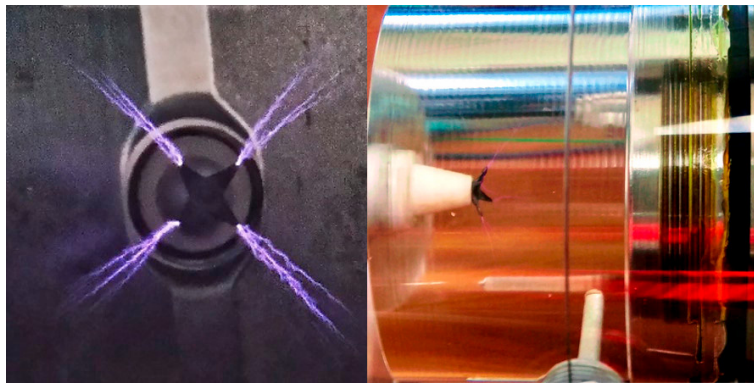

Fig. 1. Detail of the ACIS 4-tips electrode (a). Detail of the bomb chamber (b).

The conventional spark igniters are driven by an Arbitrary Wave Generator (*HP 33120A*) that triggers the spark and controls the frequency and the number of the multiple spark events [14]. The gas which fills the bomb is supplied by cylinders for its purity, since it can widely affect the behavior of the streamers (i.e., the induced plasma), in particular for the inclusion of electronegative species like oxygen [15, 16]. The medium is replaced before any test sequence.

2.2. Methodology and procedures

The oscilloscope sampling frequency is 10 *MHz*, 10 times bigger than the frequency of the ACIS current (about 1 *MHz*). The natural frequency of the pressure sensor is $\approx 13\ kHz$ and therefore it can not be used to resolve pressure components above this frequency. When the current starts, it suddenly induces electronic noise that heavily affects the pressure (fig. 2.a) and only after some tens of μs a response is visible. This delay is compatible with the traveling time of a pressure wave across the bomb at the speed of sound, from the igniter tip to the sensor. The pressure rise is quite complex, probably due to the interference of the reflecting waves and the streamers persistence.

In fig. 2.a whole ACIS, single spark and MSD events are showed. The noise heavily affects the pressure signal with many components in the frequency domain (fig. 2.b). Therefore a low-pass filter at 2 *kHz* is needed to smooth out the signal adequately. Finally, the difference between the average pressure after and before the streaming/spark event generates a pressure step ΔP.
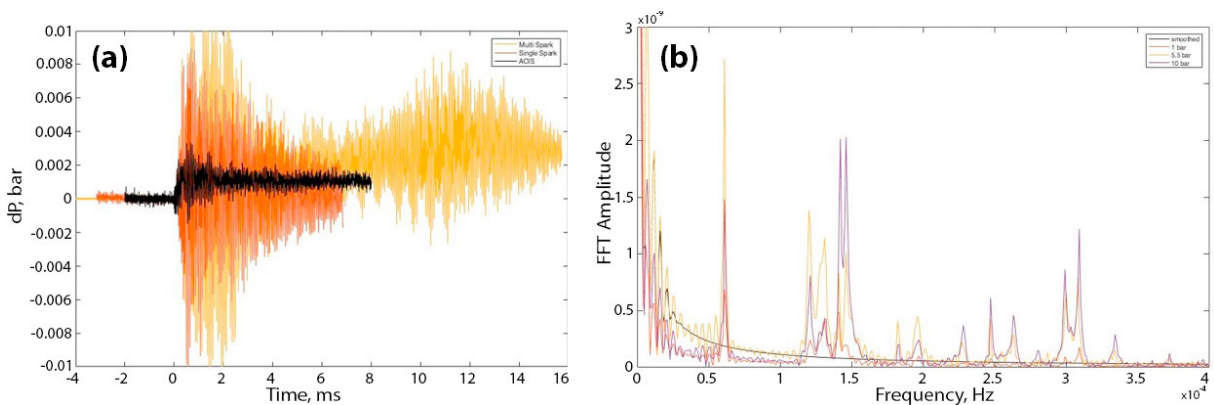

Fig. 2. Raw data acquired by the pressure sensor from three different events produced by the ACIS (black), Single Spark (red) and Multiple Spark (yellow) at $P_{chamber} = 10\ bar$ (a). ACIS frequency spectrum of the smoothed signal at 5.5*bar* (black) and of the raw signals at 1 *bar* (red), 5.5 *bar* (yellow) and 10 *bar* (purple) (b).

From the evaluated ΔP, the energy E delivered to the chamber medium is then calculated, by assuming the chamber as an adiabatic system [13], because the increase of the gas temperature during the streaming is negligible, and the chamber wall is an excellent insulator. Under these conditions, applying the first law of thermodynamics the following equation is obtained

$$E = \frac{1}{\gamma - 1} V_c \cdot \Delta P \tag{1}$$

where γ is the specific heat ratio, and V_c is the chamber volume. For each operating condition, about one hundred ΔP are collected and averaged to obtain the value of E.

3. Results and discussion

The measurements were carried out at room temperature and at increasing chamber pressure levels to take into account the pressure influence on the released energy: 1 *bar*, 5.5 *bar* (5 *bar* in the MSD test) and 10 *bar*. In the *ACIS* case, we included a sensitivity analysis on the main control parameter, i.e. the *Supply Voltage Offset* (V_{off}), that sets the input to the high frequency amplifier to properly match the energy requirement of the working conditions [9, 8].

3.1. Single Spark

The energy supplied to the primary circuit (*primary energy supplied*, E_{PS}) is almost constant during the whole recorded data-set and approximately independent of the bomb condition, near 105 *mJ* for any pressure level. Indeed, the standard deviation (σ^E_{PS}) is around 1.5 *mJ* for any pressure, larger than the difference between each E_{PS} at the various $P_{chamber}$. Data are summarized in table 1.

For each $P_{chamber}$, the thermal energy released by the spark to the medium (E_{TR}) resulted to be constant for the whole tests. The distribution of E_{TR} data series is quite variable (see σ^E_{TR} column of tab. 1, the relative σ^E_{TR} is about 17%, 9% and 17% for 1 *bar*, 5.5 *bar* and 10 *bar*, respectively) but it does not show any particular trend as the pressure increases, even if measurement conditions are limited to clearly identify a trend.
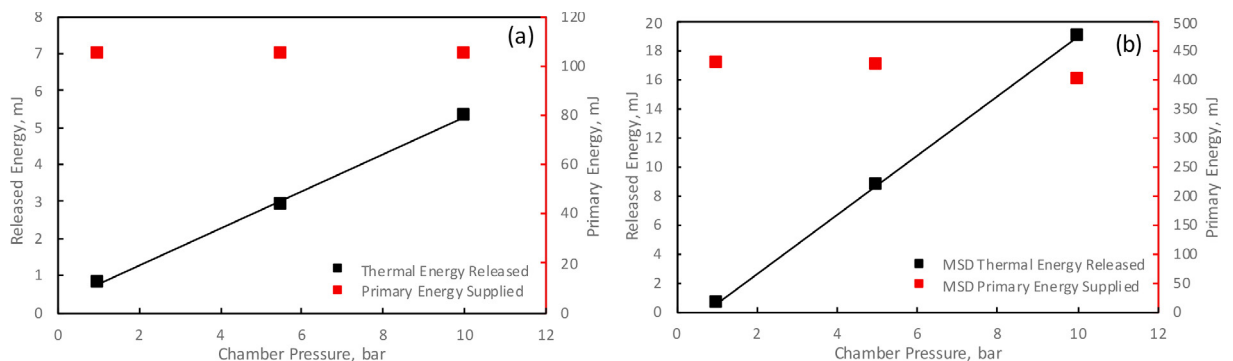

Fig. 3. Single Spark (a) and MSD (b) Ignition System: energetic assessment of the measured values for the three different bomb inner pressure $P_{chamber}$: E_{TR} (black squares) and E_{PS} (red squares).

As expected, E_{TR} depends on the chamber pressure: the higher the pressure, the larger the dielectric between the electrodes and the higher the power needed. In other words, stronger electric field is required to reach the breakdown and arc condition. The average value of the released thermal energy E_{TR} ranges from 0.83 *mJ* at ambient pressure to 5.31 *mJ* at 10 *bar*, showing an almost linear trend (fig. 3.a).

The efficiency increases as the chamber pressure increases, consistently with the released thermal energy, as the primary supplied energy is basically constant, and it reaches 5.1% at 10 *bar*. Table 1 summaries the results for the single spark case.

Table 1. Single-Spark and Multi-Spark: energy supplied to the primary circuit E_{PS}, thermal energy released in the bomb medium E_{TR}, relative standard deviation of the data distribution (σ_{PS}^E and σ_{TR}^E, respectively) and overall efficiency η_E.

Ignition System	$P_{chamber}$ [bar]	E_{PS} [mJ]	σ_{PS}^E [mJ]	E_{TR} [mJ]	σ_{TR}^E [mJ]	η_E
	1	105.1	1.6	0.83	0.14	0.8%
Single Spark	5.5	105.1	1.5	2.95	0.3	2.8%
	10	104.7	1.5	5.3	0.9	5.1%
	1	429.5	11.0	0.53	0.08	0.1%
MSD	5	424.5	5.2	8.75	0.8	2.1%
	10	401.0	9.2	19.1	1.9	4.8%

3.2. Multiple Spark

The MSD Ignition System is similar to the previous igniter as for the general features, but it produces many sparks in a short amount of time, belonging to the same event, and the energy management is therefore quite different. Fig. 4.a shows how the primary circuit is fed vs. time (E_{PS} per sample, black solid line), essentially reflecting the supply current trend during an event. The first charge is by far the most intense and longest; the first breakdown is well recognizable by the first sudden drop of the supplied energy. The breakdown characterizes the thermal energy release start (E_{TR} red line of 4.a). The released energy growth continues until a new spark recharge process starts (in E_{TR} this identifies a local maximum), beginning a new loop of the spark plug charge-discharge process. The last breakdown triggers a longer discharge and, consequently, a greater energy release phase, i.e. the last glow phase. This behaviour is in good agreement with the results of previous works on analogous ignition systems ([14, 17]).
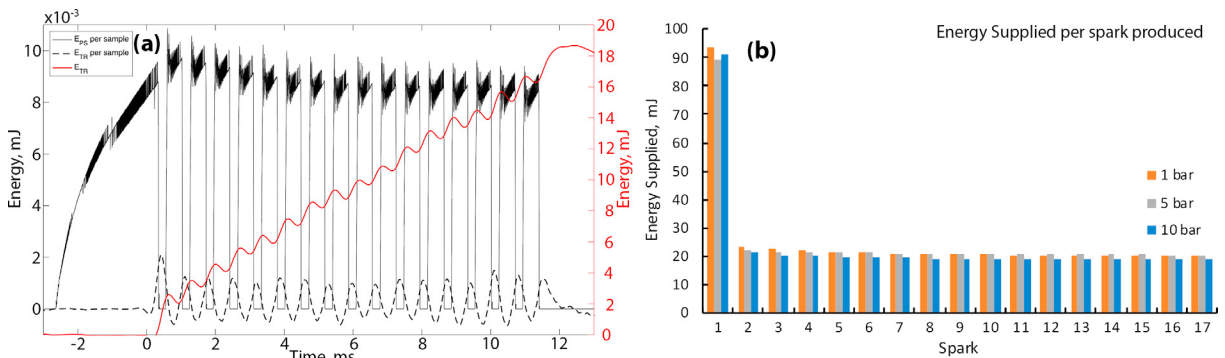

Fig. 4. Multi-spark test case. (a) example at $P_{chamber} = 10\ bar$: energy per sample supplied to the primary circuit (black solid line), thermal energy E_{TR} per sample released to the medium (black dotted line) and the overall thermal energy E_{TR} (the sum of each sample contribution, red line). (b): energy supplied to the spark plug primary circuit for each one of the 17 sparks produced by the MSD during a single event, equivalent to 17 breakdown for event.

After the breakdown, the arc and glow phases occur and require few *ms* to fully develop [13]; during these phases energy is released. In the MSD processes, a new charge-discharge loop breaks the previous arc-glow phase before it completes, except for the last breakdown.

The black dotted line of fig. 4.a represents the released thermal energy E_{TR} per sample. It is heavily affected by the data processing (in particular, by the low pass filter, see the yellow line in fig. 2.a) so that the local information is smoothed and spread out on a wider time interval. Nevertheless, it keeps track of the deposited energy amount of each spark. Each local maximum is centred on the intervals whose limits are defined by $E_{PS} = 0\ mJ$, i.e. charge and discharge are alternate; the last peak is asymmetrical, with a prolonged tail, that is due to the largest thermal energy released by the last discharge glow phase. E_{TR} per sample and E_{PS} per sample are plotted on the same axis on purpose, to allow their comparison, as their ratio is the energy efficiency.

The value of the sum of the E_{PS} per sample for each spark (fig. 4.b) is variable but the first discharge is by far the most energetic. The MSD system absorbs most of the required energy in the 3 *ms* preceding the first spark. This energy is then stored and partially refilled before each breakdown and finally dissipated with the last spark event.

The MSD showed a quite constant E_{PS} for the whole test, while it is slightly dependent on $P_{chamber}$, showing a decrease with pressure, which was negligible for the single spark. In this case, $P_{chamber}$ has an impact with such an high level of energy. The data dispersion is not so stable, but results independent of the $P_{chamber}$ (σ_{PS}^{E} column, tab. 1).

The E_{TR} follows the single spark trend, approximately linear (fig. 3,b): almost constant for the test duration and considerably affected by $P_{chamber}$, increasing quickly with $P_{chamber}$ (reaching about 19 mJ at 10 bar). The data dispersion does not affect the high pressure data distribution excessively (see σ_{TR}^{E} column in tab. 1). As expected from the E_{PS} and E_{TR} trends, the efficiency increases with the bomb pressure $P_{chamber}$. Data are summarized in tab. 1.

3.3. ACIS

The ACIS has different setting parameters that can be adjusted to modify the streamer behaviour. We took into account the main parameter V_{off} only, as exploring the full range of settings and control parameters would be beyond the scope of this work. On the other hand, the V_{off} exploration is fundamental, because it defines the power supplied to the igniter and its value is expected to be calibrated and set up for each engine operating condition [9]. Furthermore, we found there is not a common value of V_{off} that optimizes the three tested pressures of 1, 5.5 and 10 bar.

The V_{off} operating window is determined by finding the power conditions of minimum value, below which there is no streamers production, or of maximum value, above which the undesired arc condition appears and the ACIS works in spark mode [9]. The window is then divided in four intervals of about the same width. It should be noted that, while the lower limit depends on the medium density only, the upper limit is variable according the arc conditions due to $P_{chamber}$. At 1 bar the arc takes place between the igniter tip and its tip holder, while for higher pressure the arc conditions are achieved near the pressure sensor. The whole test campaign is summarized in table 2.

Table 2. ACIS results. σ_{TR} is the standard deviation of the released energy E_{TR} distribution assumed as width evaluation.

$P_{chamber}$ [bar]	V_{off} [V]	E_{PS} [mJ]	E_{TR} [mJ]	σ_{TR} [mJ]	σ_{TR} [%]	η_E
	11	42.4	0.55	0.17	31.6%	1.3%
	18	99	2.53	0.21	8.3%	2.6%
1	24	162.5	9.12	0.30	3.3%	5.6%
	30	238	20.0	0.6	2.9%	8.4%
	36	326	31.6	1.6	5%	9.7%
	32	266	0.22	0.21	93.4%	0.1%
	40	391	4.06	0.46	11.3%	1.0%
5.5	47	516	16.7	1.0	6.1%	3.2%
	54	655	43.2	5.0	11.7%	6.6%
	62	831	64.5	5.5	8.5%	7.8%
	44	460.5	0.77	0.25	31.9%	0.2%
	47	516	1.4	0.25	17.2%	0.3%
10	50	574	2.9	0.25	8.6%	0.5%
	53	634.5	5.4	0.7	13%	0.9%
	56	697.5	8.35	0.84	10.1%	1.2%

The electrical energy supplied to the ACIS igniter can be evaluated as a function of the setting parameters. $E_{PS} \propto V_{off}^{1.7208}$, independently of the applied pressure inside the bomb: the trend of this function is well visible in fig. 5.a, where all the three cases overlap.

The thermal energy released to the medium quickly increases with the voltage offset V_{off}, while the pressure increase, at constant V_{off}, reduces E_{TR}, essentially because the conditions to establish streamers become harder. The measured points lie on the fitting curve $E_{TR} \propto V_{off}^{2}$ (fig. 5.b). The growth of $P_{chamber}$ moves those curves to higher voltages; it is difficult to derive a unique law which describes the three curves. The interval width of V_{off} heavily affects the energy development. However, the trend of E_{TR} being proportional to V_{off}^{2} is well established.

The ACIS efficiency shows three different intervals, varying E_{off} (fig. 5.c):

1. low V_{off} - this interval is characterized by a slow increase, like the slow E_{TR} starting increase;
2. intermediate value of the V_{off} - it is characterized by a fast growth; in this section the increase of E_{TR} with V_{off} is much faster than the supplied energy growth E_{PS} in the same V_{off} phase;

3. high value of V_{off} - it is characterized by a new reduction of the growth rate, due to the dependence of E_{TR} and E_{PS} on the respective powers of V_{off}, namely 2 and 1.7208, such that, finally, $\eta \propto V_{off}^{0.2792}$. Of course, nothing is inferable for higher values of V_{off}.
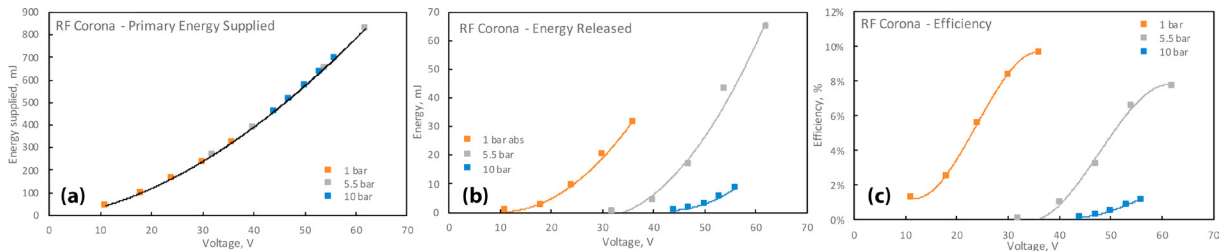

Fig. 5. ACIS; energy supplied to the primary circuit E_{PS} (a); thermal energy released to the chamber medium E_{TR} (b) a at 1 *bar* (orange), 5.5 *bar* (grey) and 10 *bar* (blue); energetic efficiency $\eta_e = E_{TR}/E_{PS}$ for the three different values of the bomb pressure $P_{chamber}$ (c).

Finally, the width of the released energy data distribution, produced by the sequence of the streamer events and estimated by the standard deviation σ_{TR} (5th column of tab. 2), shows a very light increase with V_{off}, corresponding to a pronounced relative reduction. The σ_{TR} values corresponding to the lowest V_{off} suffer from the weak and noisy signal produced by the ACIS in those operating conditions.

4. Conclusions

The measurement of the energy deposited in pure air by three different ignition systems, one of which is a low temperature plasma-assisted igniter, has been carried out at three chamber pressures. The results showed that, varying the pressure, the energy supplied to the primary circuit for the single spark system is about constant while the trend of the multiple spark case is slightly decreasing. The energy fed to the ACIS system is fully independent from the bomb inner pressure.

The second result obtained is the measurement of the thermal energy provided to the chamber medium by the ignition systems: the single and multi-spark systems showed the same increasing trend with the pressure increase. Similarly, the efficiency of these two systems to release the absorbed electric energy increases with the pressure. The ACIS thermal energy released case is a bit more complex. The pressure increase produces a marked drop in the released energy, with the same V_{off} (same energy supplied). Actually, higher V_{off} operating values are available to the ACIS system, so that the system is capable of reaching very high E_{TR} values, if compared to the spark plug system. This energy can be increased until the system reaches the undesired arc conditions, established by the geometry of the chamber. The efficiency reaches the highest levels for low pressure and has a clear trend change for the highest V_{off}, but without an actual inversion towards low values.

Therefore, in a real engine application, in principle it is possible to manage the deposited thermal energy in the working medium, by properly setting the control ACIS parameters, in particular V_{off}, depending on the operating conditions (i.e. engine point, equivalence ratio and/or EGR rate).

Further analyses will be carried out to better understand the ACIS system, in particular as a function of the different working parameters and by exposing the streamers to various gas types and pressures.

Acknowledgements

References

[1] Andrey Starikovskiy and Nickolay Aleksandrov. Plasma-assisted ignition and combustion. *Progress in Energy and Combustion Science*, 39(1): 61–110, feb 2013. ISSN 03601285. doi: 10.1016/j.pecs.2012.05.003. URL http://dx.doi.org/10.1016/j.pecs.2012.05.003http://linkinghub.elsevier.com/retrieve/pii/S0360128512000354.

[2] John Burrows and Kristapher Mixell. Analytical and Experimental Optimization of the Advanced Corona Ignition System. In Michael Günther and Marc Sens, editors, *Ignition Systems for Gasoline Engines*, volume 2, pages 267–292. Springer International Publishing, Cham, 2017. ISBN 978-3-319-45503-7. doi: 10.1007/978-3-319-45504-4_17. URL http://link.springer.com/10.1007/978-3-319-45504-4{_}17.

[3] S M Starikovskaia. Plasma assisted ignition and combustion. *Journal of Physics D: Applied Physics*, 39(16):R265–R299, aug 2006. ISSN 0022-3727. doi: 10.1088/0022-3727/39/16/R01. URL http://stacks.iop.org/0022-3727/39/R265http://stacks.iop.org/0022-3727/39/i=16/a=R01?key=crossref.978ad5eef7e6c1e79038889cadc11150.

[4] D. Singleton, S. J. Pendleton, and Martin A. Gundersen. The role of non-thermal transient plasma for enhanced flame ignition in C2H4-air. *Journal of Physics D: Applied Physics*, 44(2):022001, jan 2011. ISSN 00223727. doi: 10.1088/0022-3727/44/2/022001. URL http://stacks.iop.org/0022-3727/44/i=2/a=022001?key=crossref.7f71843701e9c11aedbdb4be72cb9047.

[5] Cherian A Idicheria and Paul M Najt. Potential of Advanced Corona Ignition System (ACIS) for Future Engine Applications. In *Ignition Systems for Gasoline Engines*, pages 315–331. Springer International Publishing, Cham, 2017. ISBN 978-3-319-45503-7. doi: 10.1007/978-3-319-45504-4_19. URL http://link.springer.com/10.1007/978-3-319-45504-4{_}19.

[6] Benjamin Matthew Wolk and Isaac Ekoto. Calorimetry and Imaging of Plasma Produced by a Pulsed Nanosecond Discharge Igniter in EGR Gases at Engine-Relevant Densities. *SAE International Journal of Engines*, 10(3):2017–01–0674, mar 2017. ISSN 1946-3944. doi: 10.4271/2017-01-0674. URL http://papers.sae.org/2017-01-0674/.

[7] Taisuke Shiraishi and Tomonori Urushihara. Fundamental Analysis of Combustion Initiation Characteristics of Low Temperature Plasma Ignition for Internal Combustion Gasoline Engine. apr 2011. doi: 10.4271/2011-01-0660. URL http://papers.sae.org/2011-01-0660/.

[8] Alessandro Cimarello, Carlo N. Grimaldi, Francesco Mariani, Michele Battistoni, and Massimo A. Dal Re. Analysis of RF Corona Ignition in Lean Operating Conditions Using an Optical Access Engine. In *SAE Technical Paper*, pages 1–22, mar 2017. doi: 10.4271/2017-01-0673. URL http://papers.sae.org/2017-01-0673/.

[9] Alessandro Cimarello, Valentino Cruccolini, Gabriele Discepoli, Michele Battistoni, Francesco Mariani, Carlo Grimaldi, and Massimo Dal Re. Combustion Behavior of an RF Corona Ignition System with Different Control Strategies. In *SAE Technical Paper*, pages 1–19, apr 2018. doi: 10.4271/2018-01-1132. URL http://www.sae.org/content/2018-01-1132/.

[10] James Sevik, Thomas Wallner, Michael Pamminger, Riccardo Scarcelli, Dan Singleton, and Jason Sanders. Extending Lean and Exhaust Gas Recirculation-Dilute Operating Limits of a Modern Gasoline Direct-Injection Engine Using a Low-Energy Transient Plasma Ignition System. *Journal of Engineering for Gas Turbines and Power*, 138(11):112807, may 2016. ISSN 0742-4795. doi: 10.1115/1.4033470. URL http://gasturbinespower.asmedigitalcollection.asme.org/article.aspx?doi=10.1115/1.4033470http://dx.doi.org/10.1115/1.4033470.

[11] Fabian Marko, Gerhard König, Tobias Schöffler, Steffen Bohne, and Friedrich Dinkelacker. Comparative Optical and Thermodynamic Investigations of High Frequency Corona- and Spark-Ignition on a CV Natural Gas Research Engine Operated with Charge Dilution by Exhaust Gas Recirculation. In *Ignition Systems for Gasoline Engines*, pages 293–314. Springer International Publishing, Cham, 2017. ISBN 978-3-319-45503-7. doi: 10.1007/978-3-319-45504-4_18. URL http://link.springer.com/10.1007/978-3-319-45504-4http://link.springer.com/10.1007/978-3-319-45504-4{_}18.

[12] Riccardo Scarcelli, Anqi Zhang, Thomas Wallner, Douglas Breden, Anand Karpatne, Laxminarayan Raja, Isaac Ekoto, and Benjamin Wolk. Multi-dimensional Modeling of Non-equilibrium Plasma for Automotive Applications. In *SAE Technical Papers*, volume 2018-April, pages 1–10, apr 2018. doi: 10.4271/2018-01-0198. URL http://www.sae.org/content/2018-01-0198/.

[13] Zainal Abidin and Christopher Chadwell. Parametric Study and Secondary Circuit Model Calibration Using Spark Calorimeter Testing. In *SAE Paper*, apr 2015. doi: 10.4271/2015-01-0778. URL http://papers.sae.org/2015-01-0778/.

[14] Claudio Poggiani, Michele Battistoni, Carlo N. Grimaldi, and Adriano Magherini. Experimental Characterization of a Multiple Spark Ignition System. *Energy Procedia*, 00:1–6, dec 2015. ISSN 18766102. doi: 10.1016/j.egypro.2015.11.887. URL http://linkinghub.elsevier.com/retrieve/pii/S1876610215026478.

[15] Sergey Leonov, Dmitry Opaits, Richard Miles, and Victor Soloviev. Time-resolved measurements of plasma-induced momentum in air and nitrogen under dielectric barrier discharge actuation. *Physics of Plasmas*, 17(11):113505, nov 2010. ISSN 1070-664X. doi: 10.1063/1.3494279. URL http://aip.scitation.org/doi/10.1063/1.3494279.

[16] C. L. Enloe, R. S. Mangina, and G. I. Font. Normalized Electronegative Species Effects in the Dielectric-Barrier-Discharge Plasma Actuator. *AIAA Journal*, 54(7):2061–2068, jul 2016. ISSN 0001-1452. doi: 10.2514/1.J054551. URL http://arc.aiaa.org/doi/10.2514/1.J054551.

[17] Claudio Poggiani, Alessandro Cimarello, Michele Battistoni, Carlo N. Grimaldi, Massimo A. Dal Re, and Matteo De Cesare. Optical Investigations on a Multiple Spark Ignition System for Lean Engine Operation. In *SAE Technical Papers*, number 2016-01-0711, apr 2016. ISBN 2016010711. doi: 10.4271/2016-01-0711. URL http://papers.sae.org/2016-01-0711/.